Article Kiran - 19-20

Physics of Fluids

Laser-driven Marangoni flow and vortex formation in a liquid droplet

Cite as: Phys. Fluids 32, 121701 (2020); https://doi.org/10.1063/5.0025469
Submitted: 19 August 2020 • Accepted: 04 November 2020 • Published Online: 02 December 2020

Krishnkumar Gupta, Kiran M. Kolwankar, Bhalchandra Gore, et al.

Physics of Fluids LETTER scitation.org/journal/phf

Laser-driven Marangoni flow and vortex formation in a liquid droplet

Cite as: Phys. Fluids 32, 121701 (2020); doi: 10.1063/5.0025469
Submitted: 19 August 2020 • Accepted: 4 November 2020 •
Published Online: 2 December 2020

Krishnkumar Gupta,[1] Kiran M. Kolwankar,[1,a)] Bhalchandra Gore,[2] Jayashree A. Dharmadhikari,[3] and Aditya K. Dharmadhikari[4,a)]

AFFILIATIONS

[1]Department of Physics, Ramniranjan Jhunjhunwala College, Mumbai 400086, India
[2]Department of Scientific Computing, Modeling & Simulation, Savitribai Phule Pune University, Pune 411 007, India
[3]Raman Research Institute, Bangalore 560080, India
[4]Department of Nuclear and Atomic Physics, Tata Institute of Fundamental Research, Mumbai 400005, India

[a)]**Authors to whom correspondence should be addressed:** kiran.kolwankar@gmail.com and aditya@tifr.res.in

ABSTRACT

We present a systematic study of the laser-driven Marangoni flow and curvature induced vortex formation in a copper sulfate pentahydrate solution, visualized by dispersed carbon nanotube (CNT) bundles. The experiments are carried out using different objectives of numerical aperture (NA) in the range of 0.1–0.6 to investigate the effect of focusing on the flow dynamics. The flow velocities measured (for 0.1 NA) are in the range of 2 mm/s–5 mm/s depending on the size of CNTs. Both primary and secondary vortices are observed in our experiment. In the primary vortex, with a sixfold increase in NA, a tenfold increase in the angular velocity of CNTs is measured. We also discuss the important role played by the curvature of the droplet in the vortex formation. The numerical simulations carried out for flow velocity are in agreement with the experimental values.

Since its discovery more than three decades ago,[1] optical tweezers are widely utilized for trapping of micrometer and nanometer size particles. However, some applications demand the confinement of many particles. There have been previous attempts to circumvent this problem by focusing a continuous wave (CW) laser in an absorbing liquid to generate and trap bubbles,[2] wherein the trapped bubbles attract nearby particles.[3,4] The gradient of temperature is necessary for such a movement.[5,6] In the case of an absorbing liquid surface, because of laser heating, non-uniform surface tension is created, giving rise to the Marangoni flow[7] that depends on its gradients. The transition from an optical to thermal trapping has been observed for polystyrene beads in a weakly absorbing medium.[8] In the case of trapped bubbles in an absorbing dye, the simulated trap strength was found to be $>5 \times 10^{-9}$ N due to the Marangoni effect.[9] Apart from liquid absorbers, gold nanoparticle based resonant surface plasmon heating has been utilized to generate bubbles; the temperature change of ~3 K gave rise to a flow velocity of ~1000 μm/s.[10] Recently, using multiple laser spots, the direction of fluid flow was controlled in an absorbing film of gold nanoislands.[11] We have shown earlier a laser-based generation of gaseous, vaporous, and mixed bubbles using carbon nanotubes (CNTs) as an absorber at a low incident power of 5 mW.[12] Furthermore, with the use of a CW 1064 nm laser, dendritic patterns and accelerated crystal growth are observed in various solutions dispersed with CNTs.[13,14]

The Marangoni effect has widespread utility in microfluidic applications; flow velocities of magnitude higher than 1000 μm/s are reported using a sharp probe attached to a heater causing a temperature change of ~1 °C in water and oil.[15] Earlier, a massive movement of polystyrene beads was demonstrated with a maximum velocity of 8 mm/s, using an infrared (1.55 μm) laser-induced vortex flow in water.[16]

Namura and co-workers, using a gold nanoparticle film, created a bubble and then moved the laser beam in its vicinity and observed two circular flows that aided in the sorting of polystyrenes spheres.[17] In a subsequent work,[18] by balancing the horizontal and vertical temperature gradient controlled by the laser position around the bubble, a nearly collimated particle flow was demonstrated. Recently,[19] the collection of graphite oxide nanoplatelets dispersed

in water was demonstrated by laser-induced bubble formation using a 980 nm wavelength.

It is known that many fluid dynamical phenomena are influenced by the geometry of the boundary or the substrate in a fashion that is not yet completely understood. Recently,[20–22] the effect of the curvature of the substrate on the Rayleigh–Taylor instability has been reported. The effect of channel geometry on the migration of droplets due to the Marangoni effect has also been studied.[23] Miyakawa and Adachi studied the effect of the air–liquid interface of a droplet on the flow of microparticles near the interface.[24]

Here, we investigate the hitherto unexplored effect focusing has on flow dynamics when a liquid drop is heated by a CW laser using microscope objectives of NA in the range of 0.1–0.6. We present our experimental and simulation results of the Marangoni flow and formation of vortices in an absorbing liquid when irradiated by a focused CW 1064 nm laser beam. The vortex formation and flow patterns are investigated by varying experimental conditions such as the incident laser power. The flow patterns within a vortex are visualized, and the velocity of flow is quantified by measuring the velocity of dispersed carbon nanotube bundles. The numerical simulations are performed using COMSOL Multiphysics[25] that provides an insight into understanding as to how the laser beam irradiation played a significant role in temperature rise and flow velocity in our measurements.

The experimental setup (see Fig. S1 and its description) consists of a 1064 nm CW laser beam that is routed with the help of mirrors into an inverted microscope, and the microscope objective focuses the laser light into the sample. The light (back-reflected) from the sample is collected with the same objective, and the images are captured using a CCD camera. The experiments are performed using the copper sulfate pentahydrate solution, which has a strong absorption at 1064 nm wavelength, at the concentration of ~0.3 g/ml. CNTs of sizes in the range of 110 nm–170 nm are dispersed in the solution to visualize the flow patterns. The absorption coefficient of the copper sulfate pentahydrate solution at 1064 nm wavelength is 1.36 cm^{-1}. The experiments are carried out using four microscope objectives (4×/0.1, 10×/0.25, 20×/0.45, and 40×/0.6), and the incident laser power was in the range of 25 mW–85 mW, measured before the microscope objective. Copper sulfate pentahydrate crystals are dissolved in deionized water and drop cast (diameter ~3 mm) on a microscope glass slide. Initially, the vertical position of the objective is adjusted to focus the laser on the slide without the droplet; this is the reference position. The vertical motion of the microscope objective is again adjusted and locked with the droplet. The maximum apex height of the droplet is measured to be ~1.2 mm, subsequently, upon shining the laser light (60 μm away from the boundary of the drop–air interface by adjusting the horizontal motion of the slide stage) inside the drop, as shown in Fig. S1; the light is absorbed by the liquid, giving rise to localized heating. The localized heating of the solution results in the temperature gradient. In our measurements, this rise in temperature sets in flow patterns that eventually give rise to the vortex formation.

We systematically analyze, in real time, the transient time-dependent growth of the flow patterns from the recorded movies. Figure 1(a) (Multimedia view) shows the time-dependent growth pattern using a 4× objective magnification.

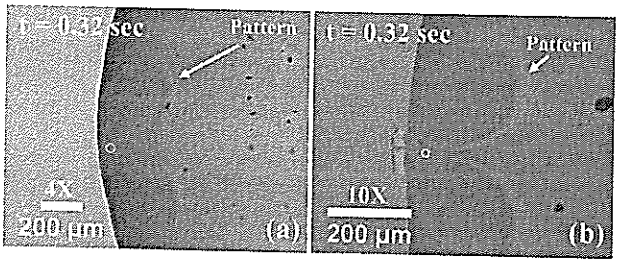

FIG. 1. Time-dependent growth of the flow pattern using (a) a 4× objective at t = 0.32 s and (b) a 10× objective at t = 0.32 s at an incident laser power of 58 mW. The open circle represents the location of a focused laser spot. Multimedia views: (a) https://doi.org/10.1063/5.0025469.1; (b) https://doi.org/10.1063/5.0025469.2

At time t = 0 s, the laser is turned on, and the beam focused inside the liquid drop. As a result, in the proximity of the laser spot, the temperature rapidly increases. A diffusion front is seen moving away from the laser spot [the white circle in Fig. 1 (Multimedia view) represents the position of the laser spot], leading to flow in the steady-state that results in the formation of primary vortices. There is a localized rise in the temperature due to the absorption of the laser radiation; subsequently, thermal currents are set up inside the liquid drop. A typical transient pattern formed in the liquid is depicted in Fig. 1(a) (Multimedia view), which then grows until the steady-state is reached (see Fig. S2). It proliferates near the laser spot (the distance from the laser spot to the droplet boundary is ~60 μm). In Fig. 1(b) (Multimedia view), we show the time-dependent growth of the pattern using a 10× objective. The laser power used in this case is 58 mW. The pattern that we observe is similar to that using a 4× microscope objective. As time progresses apart from the primary vortices, we also observe the secondary vortices. The motion of the liquid is monitored with the aid of carbon nanotubes (CNTs). The CNTs rotate in the clockwise direction in one of the vortices and the counterclockwise direction in the other vortices.

We have carried out our measurements by changing the NA. The increase in the NA leads to the increase in the temperature gradient and, hence, the increase in the Marangoni and Rayleigh numbers (see note S1 and Table 1 of the supplementary material). Hence, the measurements for different NA essentially correspond to the measurements for different Marangoni numbers. Our findings are summarized in Fig. 2. Figure 2(a) depicts the time required for the vortices to form, and Fig. 2(b) shows the time for one rotation. As can be seen, these times decrease with the Marangoni number, which is expected as with a higher Marangoni number (and ΔT), the force will be higher. Hence, the process is, in general, faster. Figure 2(c) shows that the accumulation radius decreases with the Marangoni number. This can be understood from the previous plot, which implies that the angular velocity increases with the Marangoni number. This leads to a greater centrifugal force resulting in the escape of outer particles. Figure 2(d) depicts the distance between the vortices, which decreases with the Marangoni number. This observation can be attributed to the higher velocity of the jet (see Fig. S3) between the vortices resulting in a higher pressure gradient in the direction perpendicular to the jet.

See the supplementary material for experimental and simulation details and supplementary figures.

The authors thank Professor Deepak Mathur for his encouragement during this work. They are also thankful to Shashank Pathak for assistance in the initial stages of the experiments and Anisha Kashyap for help in the programming. K.M.K. would like to thank the Science and Engineering Research Board (Grant No. EMR/2014/000255) and Council of Scientific and Industrial Research [Grant No. 03(1357)/16/EMR-II] for financial support.

DATA AVAILABILITY

The data that support the findings of this study are available from the corresponding author upon reasonable request.

REFERENCES

[1]A. Ashkin, J. M. Dziedzic, J. E. Bjorkholm, and S. Chu, "Observation of a single-beam gradient force optical trap for dielectric particles," Opt. Lett. **11**, 288–290 (1986).

[2]V. Y. Bazhenov, M. V. Vasnetsov, M. S. Soskin, and V. B. Taranenko, "Dynamics of laser-induced bubble and free-surface oscillations in an absorbing liquid," Appl. Phys. B **49**, 485–489 (1989).

[3]G. Ramanandan, A. K. Dharmadhikari, J. A. Dharmadhikari, H. Ramachandran, and D. Mathur, "Bright visible emission from carbon nanotubes spatially constrained on a micro-bubble," Opt. Express **17**, 9614–9619 (2009).

[4]H. Ramachandran, A. K. Dharmadhikari, K. Bambardekar, H. Basu, J. A. Dharmadhikari, S. Sharma, and D. Mathur, "Optical-tweezer-induced microbubbles as scavengers of carbon nanotubes," Nanotechnology **21**, 245102 (2010).

[5]K. T. Kotz, K. A. Noble, and G. W. Faris, "Optical microfluidics," Appl. Phys. Lett. **85**, 2658–2660 (2004).

[6]A. T. Ohta, A. Jamshidi, J. K. Valley, H.-Y. Hsu, and M. C. Wu, "Optically actuated thermocapillary movement of gas bubbles on an absorbing substrate," Appl. Phys. Lett. **91**, 074103 (2007).

[7]M. Gugliotti, M. S. Baptista, and M. J. Politi, "Laser-induced Marangoni convection in the presence of surfactant monolayers," Langmuir **18**, 9792–9798 (2002).

[8]P. Kumari, J. A. Dharmadhikari, A. K. Dharmadhikari, H. Basu, S. Sharma, and D. Mathur, "Optical trapping in an absorbing medium: From optical tweezing to thermal tweezing," Opt. Express **20**, 4645–4652 (2012).

[9]A. Miniewicz, C. Quintard, H. Orlikowska, and S. Bartkiewicz, "On the origin of the driving force in the Marangoni propelled gas bubble trapping mechanism," Phys. Chem. Chem. Phys. **19**, 18695–18703 (2017).

[10]K. Setoura, S. Ito, and H. Miyasaka, "Stationary bubble formation and Marangoni convection induced by CW laser heating of a single gold nanoparticle," Nanoscale **9**, 719–730 (2017).

[11]K. Namura, S. Imafuku, S. Kumar, K. Nakajima, M. Sakakura, and M. Suzuki, "Direction control of quasi-stokeslet induced by thermoplasmonic heating of a water vapor microbubble," Sci. Rep. **9**, 4770 (2019).

[12]A. K. Dharmadhikari, J. A. Dharmadhikari, A. V. Mahulkar, G. Ramanandan, H. Ramachandran, A. B. Pandit, and D. Mathur, "Dynamics of photothermally created vaporous, gaseous, and mixed microbubbles," J. Phys. Chem. C **115**, 6611–6617 (2011).

[13]H. Basu, K. M. Kolwankar, A. K. Dharmadhikari, J. A. Dharmadhikari, K. Bambardekar, S. Sharma, and D. Mathur, "Laser-driven accelerated growth of dendritic patterns in liquids," J. Phys. Chem. C **116**, 11480–11485 (2012).

[14]S. Pathak, J. A. Dharmadhikari, A. Thamizhavel, D. Mathur, and A. K. Dharmadhikari, "Growth of micro-crystals in solution by *in-situ* heating via continuous wave infrared laser light and an absorber," J. Cryst. Growth **433**, 43–47 (2016).

[15]A. S. Basu and Y. B. Gianchandani, "Shaping high-speed Marangoni flow in liquid films by microscale perturbations in surface temperature," Appl. Phys. Lett. **90**, 034102 (2007).

[16]R. Xu, H. Xin, and B. Li, "Massive assembly and migration of nanoparticles by laser-induced vortex flows," Appl. Phys. Lett. **103**, 014102 (2013).

[17]K. Namura, K. Nakajima, K. Kimura, and M. Suzuki, "Photothermally controlled Marangoni flow around a micro bubble," Appl. Phys. Lett. **106**, 043101 (2015).

[18]K. Namura, K. Nakajima, K. Kimura, and M. Suzuki, "Sheathless particle focusing in a microfluidic chamber by using the thermoplasmonic Marangoni effect," Appl. Phys. Lett. **108**, 071603 (2016).

[19]Z. Liu, J. Lei, Y. Zhang, K. Liu, W. Liu, R. Zhang, Y. Zhang, X. Yang, J. Zhang, J. Yang, and L. Yuan, "All-fiber impurity collector based on laser-induced microbubble," Opt. Commun. **439**, 308–311 (2019).

[20]P. H. Trinh, H. Kim, N. Hammoud, P. D. Howell, S. J. Chapman, and H. A. Stone, "Curvature suppresses the Rayleigh-Taylor instability," Phys. Fluids **26**, 051704 (2014).

[21]G. Balestra, P.-T. Brun, and F. Gallaire, "Rayleigh-Taylor instability under curved substrates: An optimal transient growth analysis," Phys. Rev. Fluids **1**, 083902 (2016).

[22]G. Balestra, D. M.-P. Nguyen, and F. Gallaire, "Rayleigh-Taylor instability under a spherical substrate," Phys. Rev. Fluids **3**, 084005 (2018).

[23]P. Capobianchi, M. Lappa, and M. S. N. Oliveira, "Walls and domain shape effects on the thermal Marangoni migration of three-dimensional droplets," Phys. Fluids **29**, 112102 (2017).

[24]K. Miyakawa and H. Adachi, "Laser-controlled microscale fluid flows near the air-liquid interface of suspension droplets," Phys. Rev. E **78**, 041407 (2008).

[25]COMSOL Multiphysics® V5.2, COMSOL AB, Stockholm, Sweden, (2015), www.comsol.com.

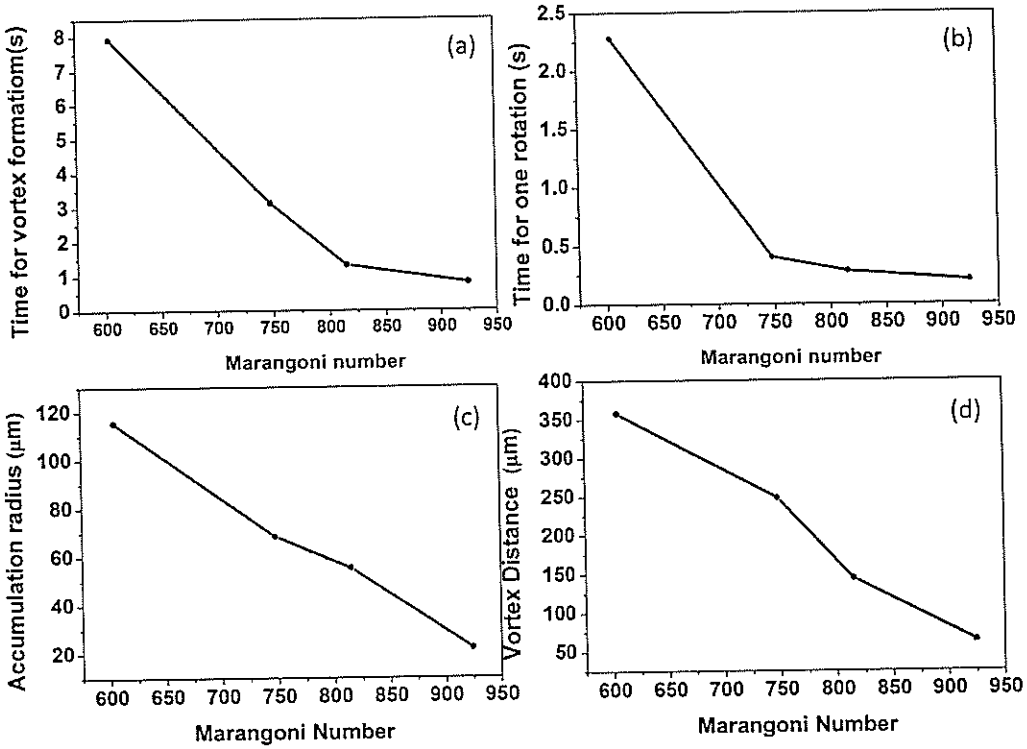

FIG. 2. Different parameters of rotational motion plotted as a function of Marangoni number for different objectives at an incident laser power of 58 mW.

The accumulated CNTs are shown (the white circle represents the position of laser spot) in Fig. 3 (Multimedia view). The images compared are at time t = 20 s after the laser is incident. The measured velocities of CNTs moving toward the vortex region are 3.2 mm/s and 2.5 mm/s for 4× and 10× magnifications, respectively. However, much higher velocities in the range of 4 mm/s–5 mm/s are measured for smaller CNTs. The maximum angular velocities of CNTs measured for the primary vortices are 8 rad/s, 55 rad/s, 58 rad/s, and 80 rad/s for 4×, 10×, 20×, and 40× magnification, respectively. We observe that a sixfold increase in the NA of the objective gives rise to a tenfold increase in the angular velocity of CNTs. Hence, it indicates that not only the angular velocity increases but also the rate of accumulation of CNTs in vortices increases with the NA of the microscope objective.

We carried out 3D simulations using a commercially available software COMSOL Multiphysics[25] for a 0.1 NA microscope objective to mimic the experimentally observed Marangoni flow and vortex formation (see note S1 of the supplementary material). We used the standard values tabulated in Table S2. The incident laser power is in the range of 25 mW–85 mW.

In Fig. 4(a), the temperature variation along the XY-plane is plotted for the incident laser power of 58 mW, focused using a 4× objective (0.1 NA). In our simulation, the laser-focused spot is located at a distance of 190 μm from the bottom surface of the

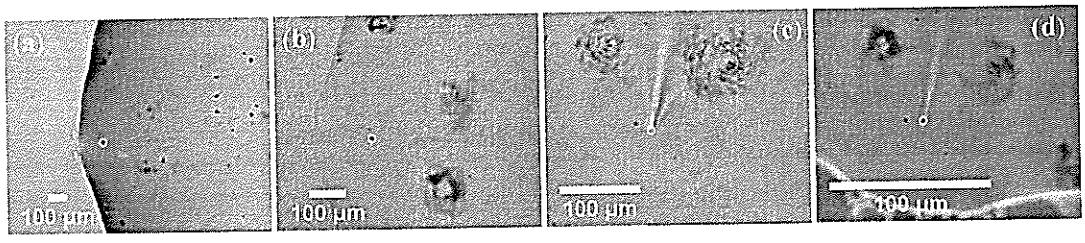

FIG. 3. Carbon nanotubes accumulation in the vortex region at t = 20 s post-laser turn on (a) 4× magnification, (b) 10× magnification, (c) 20× magnification, and (d) 40× magnification. The open white circle depicts the position of a laser focus. Multimedia view: (c) https://doi.org/10.1063/5.0025469.3

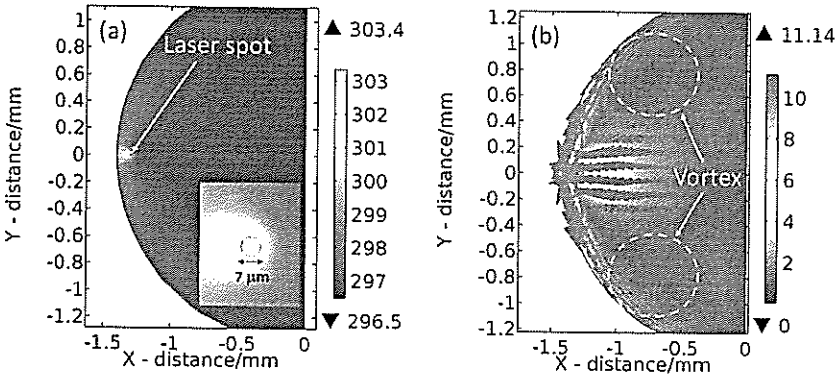

FIG. 4. (a) Temperature profile indicating the location of the focused laser spot (the color bar gives the temperature in Kelvin) and (b) velocity field in the XY-plane at 190 μm (depth of focus) from the bottom surface of the droplet. The incident laser power is 58 mW, and the radius of the laser spot is estimated to be 7 μm for a 4× microscope objective (the color bar gives the velocity in mm/s).

droplet (at a depth of focusing). The laser focus position is located at 100 μm away from the droplet boundary. Simulations are also carried out for 43 mW and 73 mW incident laser powers. It is observed that the temperature rise in the proximity of the laser focus is high, and away from the laser focus, it gradually decreases, as shown in Fig. 4(a). The change in temperature ΔT proximate to the laser spot is estimated for three different incident laser powers (see note S2 of the supplementary material). The estimated ΔT values for the 4× objective are 5.4 K, 7.2 K, and 9.1 K for 43 mW, 58 mW, and 73 mW incident laser powers, respectively. We also estimated ΔT for other objectives, and the values do not change drastically (essential for an optical control); a change in NA by a factor of 6 gives rise to a change in ΔT by a factor of ~1.5 for 43 mW incident laser power. The estimated value of ΔT at the position of the laser focus is utilized in the simulation. Earlier, we have estimated a localized temperature increase of 24 K at an incident laser power of 80 mW using a 100× objective (NA = 1.3) in hemin.[8]

The simulation results of the flow velocity and vortex formation are shown in Fig. 4(b), and the velocity field along the XY-plane is calculated at 190 μm from the bottom surface of the liquid droplet. The simulations are also performed at incident laser powers of 43 mW and 73 mW (data not shown). From Fig. 4(b), with ΔT = 7.2 K, it is evident that the velocity (represented by the arrow line) is significantly large near the laser spot, and away from the laser spot, the flow velocity has a smaller value. Moreover, away from the laser spot, a steady rotating pair of vortices (along both the sides of the heat source in a symmetric manner) is observed. The maximum flow velocity is estimated to be ~11.14 mm/s around the laser spot, and in the vortex region, the velocity is ~3.6 mm/s. In the case of 43 mW incident laser power, ΔT is 5.4 K and the maximum flow velocity is ~10.58 mm/s, and in the vortex region, the velocity has a value of ~3.2 mm/s. Likewise, for an incident laser power of 73 mW, ΔT is 9.1 K and the maximum flow velocity is ~16.2 mm/s, and in the vortex region, the velocity has a value of ~4 mm/s. When we incorporated the effect of the numerical aperture by considering different sizes of the focused laser spot inside the droplet, we did not observe a consistent change in the velocity, as observed in the experiments. In addition, we could not locate the secondary vortices observed in the experiments in our numerical simulations.

The physical origin of the vortices can be understood in the following manner. The laser beam produces a temperature gradient in bulk, leading to a convective force directed toward the laser beam inside the bulk. The laser beam also heats the surface of the drop nonuniformly creating a surface tension gradient giving rise to a Marangoni force away from the laser beam along the surface of the drop. When these forces overcome the dissipative force, a circular motion of fluid sets in, wherein the liquid travels away from the laser along the surface and again travels toward it in bulk. This argument is supported by experimental observations as well as 3D numerical simulations in a droplet like geometry. We also observe that the vortices disappear when we shift the laser beam away from the boundary, which is also seen in the simulations. This is possibly because the surface tension gradient weakens at the curved boundary. We want to emphasize that the curved nature of the boundary also plays a crucial role. This is because one needs a component of velocity directed in bulk to start the circular motion. The curvature of the boundary provides this component. We have verified this from the 3D numerical simulations by considering a rectangular boundary. The surface tension gradient along the flat boundary leads to straight-line motion along the boundary, resulting in a large scale circular motion due to another perpendicular boundary at a considerable distance. We also observe that when the drop is sandwiched between two glass plates, no vortices are formed (see Fig. S4). The absence of vortices is observed because there is no upper free surface that supports the flow away from the laser.

In summary, we have investigated the effect of focusing on the laser-based Marangoni flow and curvature induced vortex formation in an absorbing liquid droplet. The 1064 nm continuous wave laser is focused inside a stationary droplet of copper sulfate pentahydrate due to its strong absorption; a localized temperature gradient is created inside the liquid giving rise to a flow-directed outward toward a region of lower temperature. Subsequent to the directed flow, vortices are created closer to the laser-irradiated spot within the liquid. We argue that the natural convection in the bulk and the Marangoni effect along the boundary leads to these vortices. The role of curvature in the vortex formation is examined. In order to confirm our understanding, we also carried out a 3D simulation using COMSOL[27] by incorporating the Marangoni equation along with the Navier–Stokes and the heat equation. The primary vortices are reproduced, and also, the simulated velocities match satisfactorily with the experimental values. We also observe the accumulation of CNT particles that have the potential for microfluidic applications.